Evaluation of the Shear Strength of RC Beams Strengthened by Basalt Fiber Sheets

Muhaned Dawood Kashash
Department of Civil Engineering, College of Engineering, Mustansiriyah University, Baghdad, Iraq
mdk@uomustansiriyah.edu.iq (corresponding author)

Nibras Nizar Khalid
Department of Civil Engineering, College of Engineering, Mustansiriyah University, Baghdad, Iraq
nibrasnk12@uomustansiriyah.edu.iq

Received: 18 January 2025 | Revised: 11 February 2025 | Accepted: 14 February 2025

 DOI: https://doi.org/10.48084/etasr.10284

ABSTRACT

The present study experimentally investigates the use of Basalt Fiber-Reinforced Polymer (BFRP) composites for the shear strengthening of High-Strength Reinforced Concrete (HSRC) beams. The objectives of this work are to investigate the contribution of BFRP in enhancing the shear capacity and ductility of HSRC beams across different shear span-to-effective depth (a/d) ratios and to assess the effect of the number of BFRP sheet layers on shear strength improvement. The experiment involved U-wrapped 90° BFRP strips applied to HSRC beams under shear. Two groups of a/d ratios were used, namely 2.8 and 2.4. A total of eight HSRC beams with and without shear reinforcement were tested under four-point loading. The results indicate that beams with a lower a/d ratio (2.4) exhibited higher ultimate load capacities and improved shear strength compared to those with a higher a/d ratio (2.8). Specifically, for a/d 2.8, the ultimate load capacity increased by 89% with two layers of U-wrapped 90° BFRP strips, and for a/d 2.4, it increased by 49% with the same strengthening compared to the control beams. The application of BFRP U-strips significantly enhanced structural performance, increasing ultimate load capacity and reducing deflections, particularly with multiple layers.

Keywords-external strengthening; shear strengthening; fiber-reinforced polymers; basalt fiber-reinforced polymer sheets; U-shape

I. INTRODUCTION

The deterioration of concrete infrastructure due to aging along with the increasing concrete usage demands, is a global concern. Many existing Reinforced Concrete (RC) structures require strengthening and rehabilitation to extend their service life [1]. Limited maintenance budgets and steel reinforcement corrosion accelerate structural degradation [2]. Conventional retrofitting methods, such as concrete and steel jacketing, offer solutions but have drawbacks. Concrete jacketing increases structural weight and construction costs due to additional formwork, while steel jacketing involves complex welding procedures and is prone to corrosion [3]. Recent advancements in material science have introduced externally bonded Fiber-Reinforced Polymer (FRP) composites as an effective solution for structural rehabilitation [4]. Typically, unidirectional FRP wrapping sheets made of carbon, glass, or aramid fibers are used to reinforce concrete [5]. However, these conventional FRP systems are limited by their high production costs, durability issues in harsh environments, and complex installation procedures.

Over the past few decades, basalt has emerged as a promising alternative due to its favorable physicochemical and mechanical properties, cost-effectiveness, and environmentally friendly production process [6]. Its production is simple and generates lower levels of emissions and waste, as basalt is a naturally occurring material that is inherently more recyclable than synthetic strengthening. Notably, the fabrication of basalt fibers requires minimal chemical additives, solvents, or pigments - the raw basalt is simply washed and melted. Furthermore, basalt's abundance, constituting over 90% of all magmatic rocks on Earth, results in extremely low raw material costs, accounting for just 5–7% of total production expenses [7]. As a result, basalt fabrics cost approximately 20% of carbon fiber fabrics [8]. Moreover, basalt fibers exhibit superior strength, ductility, and resistance to harsh environments (alkaline, acidic, and saline) [7, 9, 10]. Additionally, basalt fiber demonstrates exceptional thermal and mechanical stability, rendering it an effective insulating material [11]. Unlike carbon fiber, basalt is electrically non-conductive, allowing safe use with metals without the risk of galvanic corrosion [7].

Building on these findings, several studies have evaluated the effectiveness of BFRP composites for the shear strengthening of RC beams. For example, authors in [12] conducted an experimental study on the effectiveness of BFRP

composites for the shear strengthening of RC beams. The study found that the failure load of the strengthened beams increased by 17-50% compared to the unstrengthened control beam/beams, with toughness enhanced by up to 2.74 times. Basalt fiber sheets demonstrated 20% higher effectiveness in increasing shear capacity compared to glass fiber sheets. The enhancement in shear capacity decreased with an increase in the preload level. Authors in [13] also investigated the shear strengthening of RC beams using BFRP composites, showing significant improvements in shear load-carrying capacity, ranging from 43% to 100%, for the BFRP-strengthened beams compared to the control specimens. The Fully Wrapped Complete Strip with 90° angle (FWCS90) and the Fully Wrapped Strips with 45° angle (FWS45) exhibited the highest enhancements in shear strength. Authors in [14] conducted an experimental and numerical study on the shear behavior of RC beams strengthened with externally bonded BFRP sheets, showing that they significantly increased the shear capacity and ductility of the RC beams.

However, despite these promising results, a comprehensive understanding of how critical parameters, such as the a/d ratio, the high strength of concrete employed, and the number of BFRP layers, affect the shear performance of RC beams remains limited. The present study addresses this gap by systematically evaluating RC beams strengthened with BFRP composites using U-wrapped 90° strips. The findings are expected to contribute to improved design guidelines and practical applications, ultimately enhancing structural performance, safety, and sustainability.

II. EXPERIMENTAL WORK

A. Overview of Experimental Specimens

This study examined eight high-strength RC beams to assess the impact of basalt fiber sheet strengthening on shear strength. Each beam was designed with dimensions of 150 mm in width, 200 mm in depth, and 1200 mm in length. The concrete cover was 20 mm and the beams were reinforced longitudinally with 16 mm diameter steel bars with no transverse reinforcement. Four beams underwent external strengthening with basalt fiber sheets, carefully applied to determine their effectiveness in improving shear strength. Two beams were designed with shear reinforcement using stirrups placed at 80 mm spacing. Figure 1 illustrates the reinforcement details, and Table I presents the data on the test matrix, including a/d ratios and basalt fiber wrapping configurations for all eight beam specimens.

B. Materials Preparation and Testing Procedure

High-strength concrete was produced using Ordinary Portland Cement (OPC) based on Iraqi Standard No. 5/1984 [15], natural sand, and 12 mm crushed gravel, both based on Iraqi Specification No. 45/1984 [16]. Micro-silica was added to improve the strength and durability in compliance with ASTM C1240/05 [17], alongside a polycarboxylate-based superplasticizer in compliance with ASTM C494/C494M-99a [18] to enhance the workability. Reinforcement included Ø 4 mm and Ø 16 mm deformed steel bars with yield strengths of 471 MPa and 522 MPa, and tensile strengths of 597 MPa and 660 MPa, respectively. Basalt fiber sheets (0.146 mm thick, tensile strength 2100 MPa, elastic modulus 105 GPa, elongation 2.6%) were bonded with epoxy resin for external strengthening.

The mixing process involved dry-mixing aggregates with cement, then gradually adding diluted superplasticizer and silica fume in a 0.04 m³ mixer. Concrete was cast in wooden molds, compacted by vibration, and cured in water at 20°C for 28 days to ensure optimal strength development.

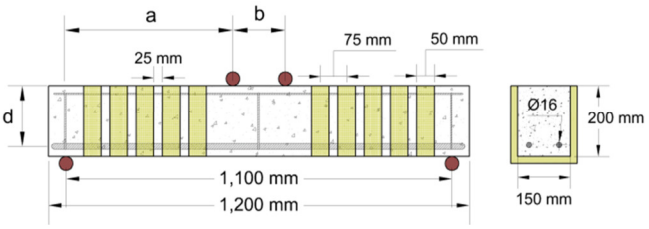

Fig. 1. Schematic of the basalt fiber sheet strengthening.

TABLE I. EXPERIMENTAL DETAILS

Beam specimen*	Shear strengthening configuration	Number of BFRP layers	The strips (width × length) mm
a/d ratio=2.8			
B_0-S_0-R2.8	Without stirrups (reference)	-	-
B_0-S_1-R2.8	With stirrups	-	-
BS_2-S_0-R2.8	BFRP U-wrapping 90˚ strips	2	50 × 550
BS_4-S_0-R2.8	BFRP U-wrapping 90˚ strips	4	50 × 550
a/d ratio=2.4			
B_0-S_0-R2.4	Without stirrups (reference)	-	-
B_0-S_1-R2.4	With stirrups	-	-
BS_2-S_0-R2.4	BFRP U-wrapping 90˚ strips	2	50 × 550
BS_4-S_0-R2.4	BFRP U-wrapping 90˚ strips	4	50 × 550

*All strengthened specimens are without stirrups.

C. Bonding Basalt Fiber-Reinforced Polymer Sheets to Concrete

Before the application of BFRP sheets, a series of preparations were carried out on the concrete surface. These included grinding to expose the coarse aggregates, according to ACI Committee 440.2R-17 [19], rounding the beam corners to a minimum 13 mm radius to prevent stress concentration, and thorough cleaning with water and acetone to remove debris and grease. A two-component epoxy adhesive, Sikadur-330, was mixed according to the manufacturer's instructions and applied as a primer on the prepared surface using a brush or roller. BFRP sheets, cut to the appropriate size, were placed on the epoxy-coated surface and further impregnated with epoxy using a roller. The epoxy-infused BFRP sheets were firmly rolled to expel air and ensure complete adhesion to the

concrete. After application, the beams were left to cure at room temperature for at least 7 days, allowing the epoxy resin to fully harden. Consistent procedures were maintained throughout the bonding process to ensure optimal performance at the interface between the BFRP composite and concrete, as depicted in Figure 2.

D. Experimental Setup

The testing on the specimens was conducted using a symmetrical four-point load system. A hydraulic universal testing apparatus (MFL system) with a maximum load capacity of 3000 kN was employed to apply the load. Two different a/d ratio values were utilized. Three Linear Variable Differential Transducers (LVDTs) were placed at the mid-span of the specimen and beneath the loads to measure the downward deflections. The schematic details of basalt fiber strengthening along with the experimental setup are illustrated in Figure 3.

Fig. 2. Enhancing concrete: bonding BFRP sheets for strengthening.

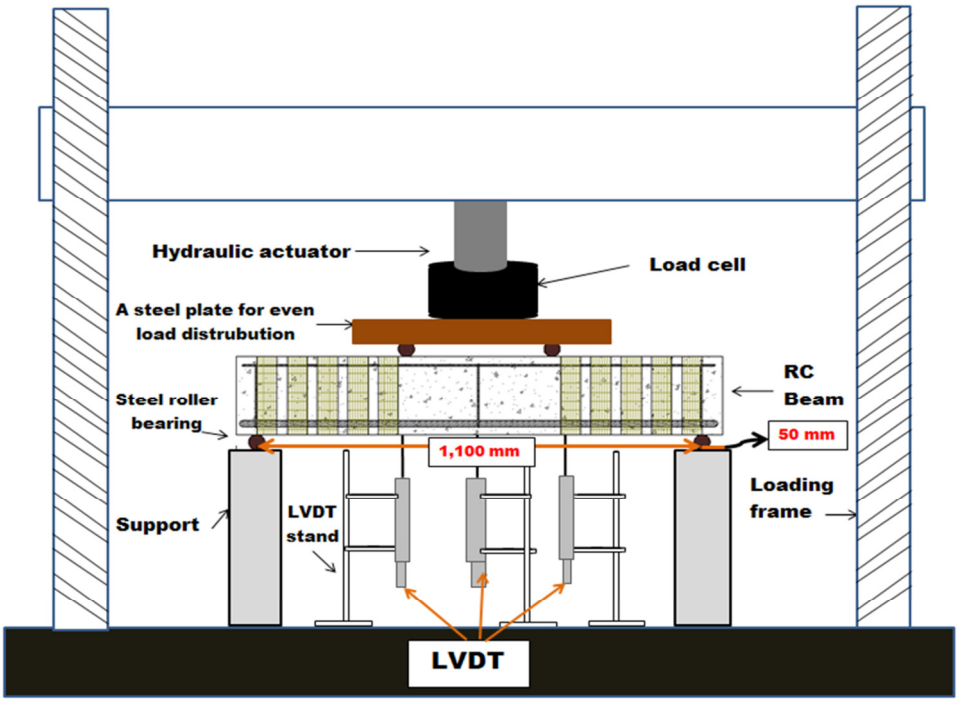

Fig. 3. Experimental load setup.

III. RESULTS AND DISCUSSION

A. Ultimate Loads

Summarized in Table II, the results provide the ultimate load capacity, which is a critical measure of the shear strength and structural performance of RC beams. In this study, an investigation was conducted to examine the effect of the a/d ratio on the ultimate load capacity of beams externally reinforced with BFRP, as shown in Figure 4. Beams without stirrups, such as the control beam B_0-S_0-R2.8, exhibited the lowest ultimate load-carrying capacity (75 kN) among all tested specimens due to a brittle shear failure mode once the concrete's shear strength was exceeded. This behavior highlights sudden and without warning shear failures.

The addition of conventional steel stirrups (B_0-S_1-R2.8) significantly increased the ultimate load capacity by approximately 102% to 153 kN. Reinforcing the beam with two layers of BFRP strips (BS_2-S_0-R2.8) resulted in an 89 % increase in ultimate load compared to the unreinforced control beam, reaching 143 kN. Further increasing the BFRP strengthening to four layers (BS_4-S_0-R2.8) led to the second highest ultimate load of 149 kN, representing a 99% increase

over the control beam. The control beam without stirrups (B_0-S_0-R2.4) exhibited an ultimate load of 105 kN, which serves as the baseline for comparison. The addition of conventional steel stirrups (B_0-S_1-R2.4) significantly increased the ultimate load capacity by approximately 71% to 179 kN. Reinforcing the beam with two layers of BFRP strips (BS_2-S_0-R2.4) resulted in a 49% increase in ultimate load compared to the unreinforced control beam, reaching 157 kN. Further increasing the BFRP strengthening to four layers (BS_4-S_0-R2.4) led to the second-highest ultimate load of 175 kN, representing a 67% increase over the control beam. The influence of a/d on the behavior of the beams was also observed. Beams with a/d = 2.4 generally exhibited higher ultimate loads and larger deflections at failure compared to the specimen with a/d = 2.8. This can be attributed to the fact that a lower a/d ratio results in more favorable shear force distribution and reduced failure of beams under shear.

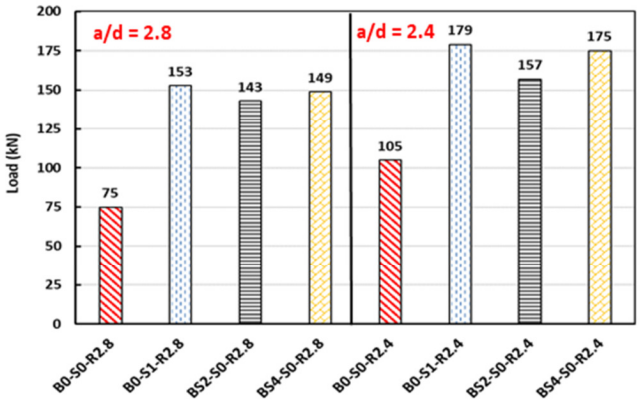

Fig. 4. Comparative analysis of ultimate load capacities in reference RC beams vs. BFRP-reinforced RC beams at different a/d ratios.

TABLE II. TEST RESULTS

Beam specimen	Ultimate load (kN)	Deflection at ultimate load (mm)	Load at first crack (kN)	Percent increase over control %	Failure mode
a/d ratio = 2.8					
B_0-S_0-R2.8	75	3.05	32	-	Diagonal tension failure
B_0-S_1-R2.8	153	6.37	22	102	Diagonal tension failure
BS_2-S_0-R2.8	143	9.34	34	89	Shear + concrete crushing failure with intact fiber bonding
BS_4-S_0-R2.8	149	7.41	40	99	Shear + debonding
a/d ratio = 2.4					
B_0-S_0-R2.4	105	3.97	30	-	Diagonal tension failure
B_0-S_1-R2.4	179	10.8	33	71	Shear - compression failure
BS_2-S_0-R2.4	157	5.17	30	49	Shear + rupture
BS_4-S_0-R2.4	175	13.8	38	67	Shear + rupture
f'_c : Cylinder Concrete Compressive Strength (Average) = 65 MPa					

B. Load-Deflection Relationship

The load-deflection behavior of the examined beams is illustrated in Figures 5-11. In Figure 5, the control beams without stirrups denoted as B_0-S_0-R2.4 and B_0-S_0-R2.8, exhibit the highest deflections among the tested configurations under their respective loads, indicating lower stiffness and a greater propensity for deformation. This is particularly noticeable as a/d increases, resulting in even higher deflections and a less stiff response.

The beams with stirrups B_0-S_1-R2.4 and B_0-S_1-R2.8 experience reduced deflections under the same loads compared to the control beams. The presence of stirrups enhances the stiffness and load capacity of the beams, effectively confining the concrete and delaying the onset of shear cracks, which results in a more ductile failure mode, as shown in Figures 6 and 7.

The application of BFRP U-strips further modifies the load-deflection behavior. Beams with 2 layers of BFRP U-strips without stirrups (BS_2-S_0-R2.4 and BS_2-S_0-R2.8) exhibit lower deflections compared to the control beams. The U-strip configuration provides additional confinement and flexural strengthening, enhancing the overall stiffness of the beams. This improvement is evident in Figures 8 and 9, where the deflections are significantly reduced, especially in beams with a lower a/d ratio.

Increasing the number of BFRP layers to 4 (BS_4-S_0-R2.4 and BS_4-S_0-R2.8), the beams show greater stiffness, resulting in further reduced deflections under the same load conditions. The increased number of layers enhances confinement and flexural strength. Figures 10 and 11 display these improvements, where the deflections are minimized, indicating the effectiveness of the additional BFRP layers.

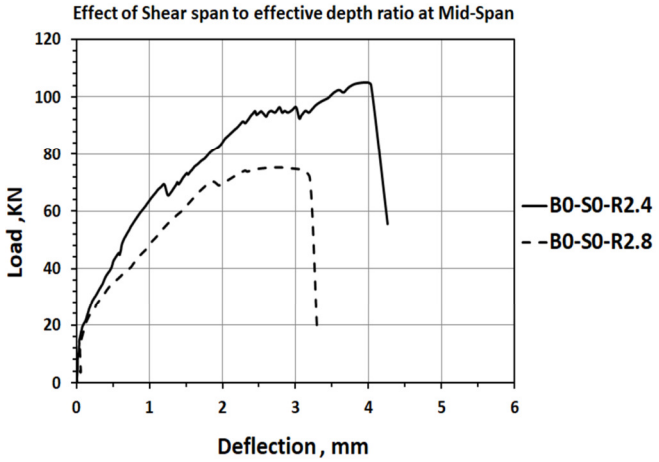

Fig. 5. Load-deflection curves of control RC beams without stirrups at ratios 2.4 and 2.8.

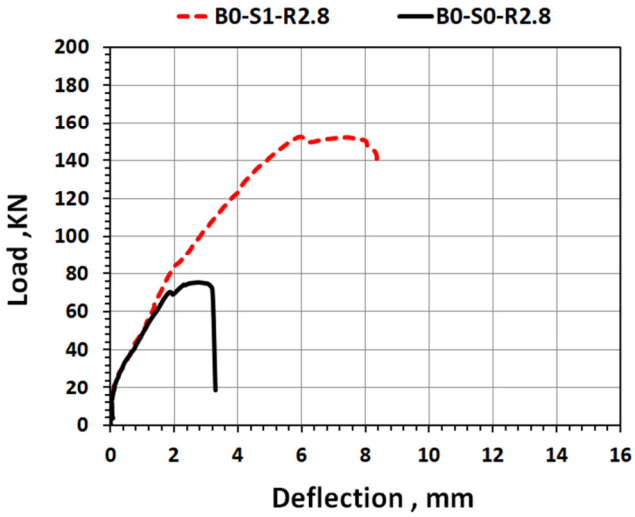

Fig. 6. Load-deflection curves of RC beams with stirrups at ratio 2.8.

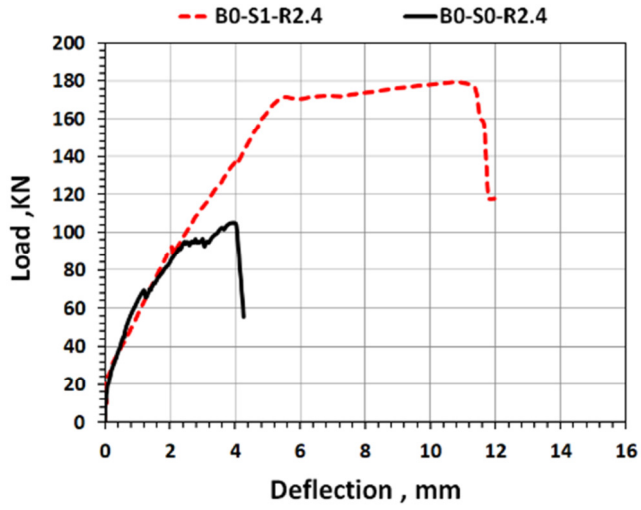

Fig. 7. Load-deflection curves of RC beams with stirrups at ratio 2.4.

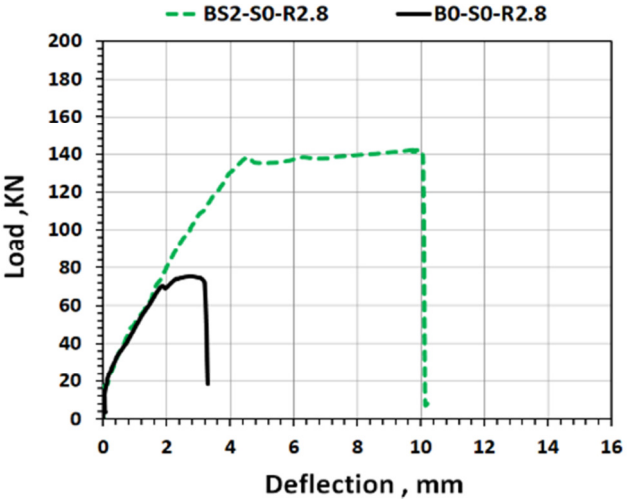

Fig. 8. Load-deflection curves of RC beams with 2 layers of BFRP U-strips without stirrups at ratio 2.8.

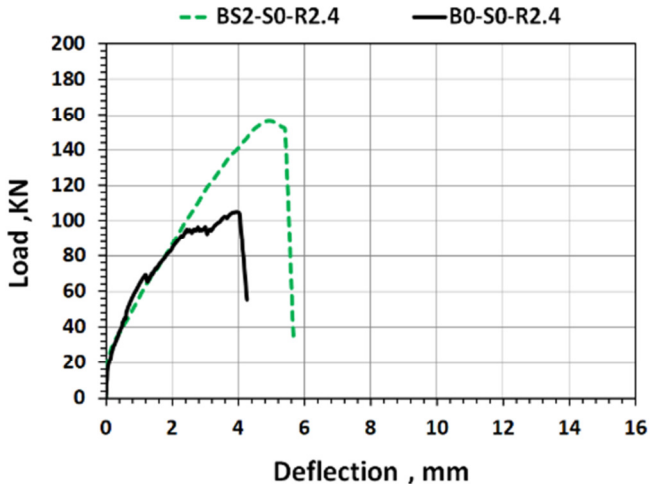

Fig. 9. Load-deflection curves of RC beams with 2 layers of BFRP U-strips without stirrups at ratio 2.4.

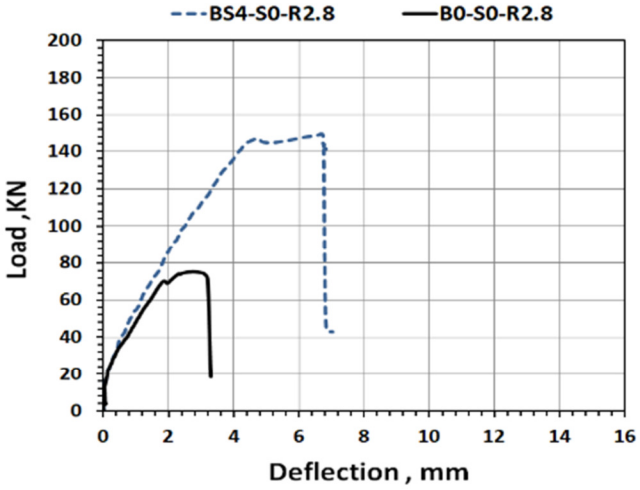

Fig. 10. Load-deflection curves of RC beams with 4 layers of BFRP at ratio 2.8.

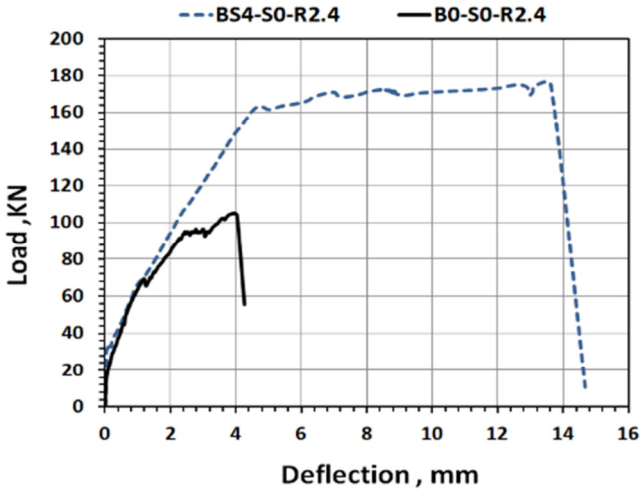

Fig. 11. Load-deflection curves of RC beams with 4 layers of BFRP at ratio 2.4.

C. Modes of Failure

The cracking patterns of the tested beams are presented in Figures 12 and 13. At the early stages of loading, several cracks appeared on the tension face within the constant maximum moment region, which is the middle portion of the beam between the two-point loads. All beams failed along the line connecting the support and the point of loading. This failure mechanism is referred to as "Diagonal Tension Shear Failure," except for one beam (B_0-S_1-R2.4), which exhibited "Shear-Compression Failure". In the control beam, the failure transpired abruptly and without any warning. This was marked by the emergence of an inclined crack accompanied by a loud sound, after which the load ceased to increase. For the external strengthening of reinforced beams using U-shaped basalt fiber strips, all beams exhibited shear and debonding failure, except for one beam which exhibited shear and concrete crushing failure with intact fiber bonding (BS_2-S_0-R2.8).

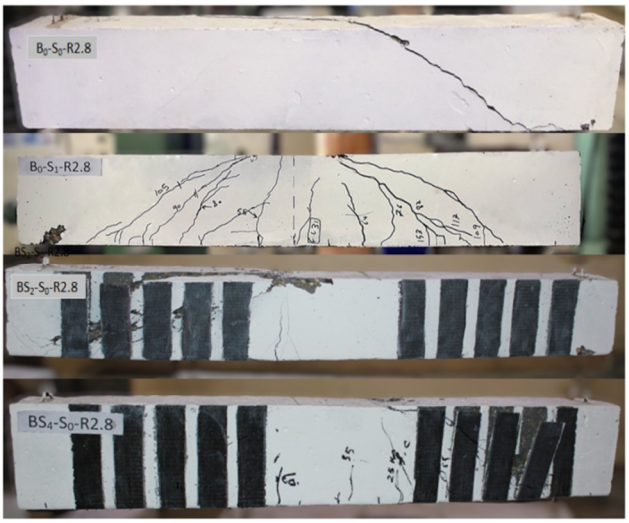

Fig. 12. Cracking patterns of the tested beams at ratio 2.8.

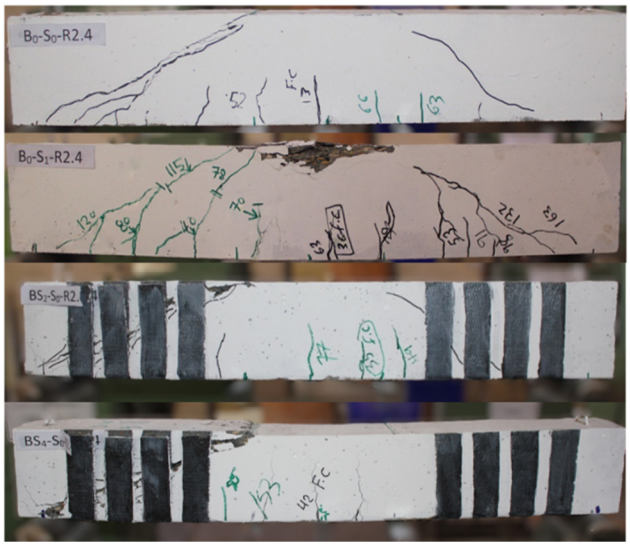

Fig. 13. Cracking patterns of the tested beams at ratio 2.4.

IV. THEORETICAL EVALUATION OF SHEAR CAPACITY IN BFRP-STRENGTHENED REINFORCED CONCRETE BEAMS

A. Theoretical Studies

Various methods have been applied for the shear strengthening of RC beams using FRP systems. Among these, certain techniques have gained widespread acceptance and are integrated into design regulations and guidelines. The most commonly adopted configurations for shear strengthening are side bonding, U-jacketing, and full wrapping. These methods are primarily employed to enhance the shear capacity of rectangular beams, as detailed in [13]. Key contributions include the design guidelines specified in ACI 440.2R-17 [19], the models proposed by Chen and Teng in [20, 21] and Khalifa et al [22], fib14 [23], and ISIS Canada Module 4 [24]. These models and equations are summarized in Table III for comparative analysis.

The shear strength of RC beams strengthened with FRP materials is typically calculated by adding the contributions from three sources: the FRP external shear strengthening, the concrete, and the internal reinforcing steel. This relationship is expressed in:

$$v_n = \emptyset \left(v_c + v_s + \psi_f v_f\right) \quad (1)$$

The ACI 440.22R-17 guidelines recommend applying an additional reduction factor, ψ_f to the FRP contribution. The terms V_C and V_s represent the shear contributions from the concrete and the internal reinforcing steel, respectively. The reduction factor ψ_f specified in ACI 440.22R-17 varies based on the FRP configuration: it is 0.95 for fully wrapped members and 0.85 for U-wrapped or side-bonded configurations. The contribution of FRP strengthening to the overall shear strength V_f is determined by using (2). The area of the FRP external strengthening A_{vf} and the effective stress f_{fe}, which represents the level of stress achieved at section failure, are calculated using (3) and (4), respectively. For the U-wrapping and two-side bonding configurations, the strain value must not exceed the limit specified in (5). The bond-reduction coefficient K_v can be calculated using (6-8). Furthermore, it is important to note that in the case of continuous fiber wrapping, the FRP spacing S_f should match the fiber width w_f, as indicated in (9). According to the fib14 model [23], the shear strengthening of RC beams requires assessing the shear capacity of the strengthened element, as outlined in (10)**.** This evaluation considers the specific contributions of side-bonded or U-shaped FRP jackets, while the effective FRP strain $\varepsilon_{f,e}$ is calculated using (11). The FRP strengthening ratio ρ_f for continuously bonded shear reinforcement with a thickness t_f is derived from (12). For the FRP strengthening to be applied in the form of sheets or strips with width b_w and spacing S_f, ρ_f is determined using (13). Additionally, the elastic modulus of the FRP E_{fu} is defined in the principal fiber direction and is measured in GPa.

The ISIS Canada Module 4 [24] provides practical guidelines for the shear strengthening of RC beams using externally bonded FRP systems, with a focus on U-wraps and

full wrapping techniques. U-wraps are highlighted for their effectiveness in beams by acting as transverse reinforcement, like steel stirrups. The module emphasizes proper anchorage of U-wraps into the compression zone to avoid premature debonding, achieved through horizontal FRP strips or alternative methods. Additionally, the rounding of beam corners to a 15 mm radius is proposed to minimize stress concentrations and enhance FRP-to-concrete load transfer. The FRP contribution is calculated using (14), with the FRP cross-sectional area defined in (15). To ensure durability and crack control, the effective strain in FRP ε_{frpe} is capped at 0.004, as shown in (16). The reduction factor R which accounts for concrete compressive strength and FRP stiffness, is determined utilizing (17-18). Additional limits on effective strain for bonded FRP systems are provided in (19-22). The spacing of FRP strips is further constrained to ensure optimal crack interception, as described in (23). Authors in [20-21] proposed a model to predict the shear contribution of FRP systems in U-wraps, side strips, and fully wrapped beams, focusing on the influence of the critical shear crack inclined at 45° to the beam's axis. The total FRP shear resistance V_{FRP} is expressed in (24), incorporating effective FRP stress, strip geometry, and spacing. The effective stress in FRP $f_{FRP,e}$ is determined using a stress distribution factor D_{FRP} and the maximum debonding stress $\sigma_{FRP,max}$, as shown in (25-29). The bond length and strip width influence the stress distribution, with the normalized bond length λ and effective bond length L_e calculated using (30-31). Authors in [22] developed a comprehensive model to estimate the shear contribution of externally bonded FRP systems for RC beams under various configurations, including U-jacketing, side bonding, and full wrapping. The shear contribution of the FRP v_f is calculated using (32), which integrates the FRP area, effective stress, and fiber inclination. A critical distinction in their model is the definition of effective stress in FRP f_{fe} determined by applying a reduction factor R in (33). The reduction factor is derived as the minimum value among three limits: the rupture limit, expressed as a polynomial equation in (34), the bond mechanism limit in (35), and the practical limit, set conservatively at 0.5 in (36). Furthermore, the model adjusts the effective FRP width and anchorage length based on the configuration, where anchorage length is determined using (37). This model ensures a conservative and reliable prediction of FRP shear contribution by incorporating stress reductions due to rupture, bonding performance, and practical design constraints.

B. Theoretical Results

The contribution of BFRP to the shear capacity $V_f(exp)$ was determined by subtracting the shear strength of the control beams from that of the beams strengthened with BFRP composites. The evaluation of shear contribution V_f in BFRP-strengthened beams, as illustrated in Figure 14 and detailed in Table IV, focuses on U-wrapped configurations with two and four layers of BFRP strengthening and a/d ratios of 2.4 and 2.8. A comparative analysis is conducted using five prediction models: Model 1 (ACI 440.2R-17) [19], Model 2 (fib14) [23], Model 3 (ISIS Canada Module 4) [24], Model 4 (Chen and Teng) [20-21], and Model 5 (Khalifa et al.)[22].

The results indicate that the number of BFRP layers significantly affects shear capacity. For beams with two layers of BFRP, the models generally perform well, with Model 2 showing the highest accuracy. For instance, for beam BS_2–S_0–R2.8, $(V_f(exp)/V_f(pred))$ is 1.1, indicating a close match with the experimental results. However, for beams with four layers, variability increases among the models. Model 1 becomes notably unconservative, particularly for BS_4–S_0–R2.4 with $(V_f(exp)/V_f(pred))$ being 0.75, raising concerns about its reliability at higher reinforcement levels. Conversely, Model 3 provides conservative predictions consistently, such as for the same beam, $(V_f(exp)/V_f(pred))$ which is 1.3, ensuring safety, but at the cost of overestimating the required reinforcement. The a/d ratio also significantly influences shear behavior. Beams with higher ratios (a/d=2.8) exhibit more flexural-dominated behavior, reducing shear reliance on BFRP strengthening. Model 1 and Model 2 perform reliably, as seen in beams BS_2–S_0–R2.8 and BS_4–S_0–R2.8. In contrast, beams with lower ratios (a/d=2.8) experience higher shear stress, requiring greater accuracy in prediction models. Under these conditions, Model 3 remains conservative, while Model 4 tends to underpredict shear strength, as evidenced by a ratio of 0.66 for beam BS_4–S_0–R2.4.

These findings emphasize the importance of model calibration to accommodate varying geometry, strengthening configurations, and shear span-to-depth ratios for accurate and reliable shear strength predictions.

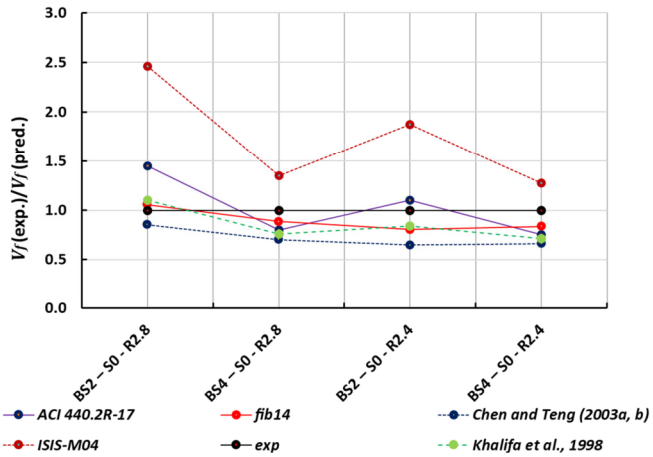

Fig. 14. Comparison between experimental and predicted BFRP shear.

V. CONCLUSION

This study demonstrates the effectiveness of different shear reinforcement strategies in enhancing the structural performance of concrete beams, particularly with steel stirrups and Basalt Fiber-Reinforced Polymer (BFRP) U-strips. Control beams without shear reinforcement exhibited the lowest load capacity, with beam B_0-S_0-R2.8 reaching 75 kN, highlighting their vulnerability to shear failure. The inclusion of steel stirrups significantly improved load-bearing capacity, increasing it by 102% to 153 kN. Similarly, strengthening with BFRP U-strips was effective, as the two layers improved capacity by 89% (143 kN) and the four layers by 99% (149 kN). Beams with a shear span-to-effective depth (a/d) ratio

ratio of 2.4 exhibited higher load capacity, with the control beam reaching 105 kN. Steel stirrups boosted this by 71% (179 kN), while two and four layers of BFRP improved it by 49% (157 kN) and 67% (175 kN), respectively. This research contributes by demonstrating that BFRP U-strips can achieve comparable or even superior strength improvements while also reducing deflections and increasing stiffness. The study also reveals that failure modes differ between reinforcement strategies, in that control beams failed suddenly by diagonal shear cracking, while BFRP-reinforced beams experienced debonding, except for BS_2-S_0-R2.8, which failed by a combination of shear and concrete crushing. This distinction in failure behavior highlights the need for further investigation into optimizing BFRP applications to prevent premature debonding. A comparative evaluation of predictive models indicates that Model 2 [23] provides accurate estimates of shear capacity in BFRP-strengthened beams, while Model 3 [24] is conservative and ensures safety. In contrast, Model 1 [19] underestimates the shear capacity of beams with high BFRP strengthening levels, suggesting potential limitations in its applicability. Further research is needed on long-term durability, hybrid strategies, debonding prevention, and predictive modeling to enhance design reliability and adoption.

TABLE III. PREDICTION OF SHEAR STRENGTH PROVIDED BY FRP

Comments	Continuous sheet	U-wraps (strips) + side bonding	General expression	Design guide
Model 1 [19]	$V_f = \frac{A_{vf} f_{fe}(sina+cosa)d_{fv}}{s_f}$ (2) $A_{vf} = 2nt_f w_f$ (3) $f_{fe} = \varepsilon_{fe} E_f$ (4)	$\varepsilon_{fe} = k_v \varepsilon_{fu} \leq 0.004$ (4) $k_v = \frac{k_1 k_2 L_e}{11{,}900\varepsilon_{fu}} \leq 0.75$ (5) $L_e = \frac{23{,}300}{(n_f t_f E_f)^{0.58}}$ (6) $k_1 = \left(\frac{f'_c}{27}\right)^{2/3}$ (7) $k_2 = \begin{cases} \frac{d_{fv}-L_e}{d_{fv}} \; for\; U \\ \frac{d_{fv}-L_e}{d_{fv}} \; for\; SB \end{cases}$ (8)	$s_f = w_f$ (9)	$v_s + v_f \leq 0.66\sqrt{f'_c} b_w d$
Model 2 [23]	$V_{fd} = 0.9\varepsilon_{f,e} E_{fu} \rho_f b_w d(cot\theta + cota)sina$ (10)	$\varepsilon_{f,e} = min \begin{cases} 0.65\left(\frac{f_{cm}^{2/3}}{E_{fu}\rho_f}\right)^{0.56} \cdot 10^{-3} \\ 0.17\left(\frac{f_{cm}^{2/3}}{E_{fu}\rho_f}\right)^{0.30} \\ \varepsilon_{fu} \end{cases}$ (11) $\rho_f = \left(\frac{2t_f}{b_w}\right)\left(\frac{b_f}{s_f}\right)$ (12)	$\rho_f = \frac{2t_f sina}{b_w}$ (13)	$E_{fu}\,(GPa)$
Model 3 [24]	$V_{frp} = \frac{\emptyset_{frp} A_{frp} E_{frp} \varepsilon_{frp} d_{frp}(sin\beta+cos\beta)}{s_{frp}}$ (14) $A_{frp} = 2t_{frp} w_{frp}$ (15) $\varepsilon_{frpe} = R \cdot \varepsilon_{frpu} \leq 0.004$ (16)	$\rho_{frp} = \left(\frac{2t_{frp}}{b_w}\right)\left(\frac{w_{frp}}{s_{frp}}\right)$ (18) $\varepsilon_{frpe} = \frac{\alpha k_1 k_2 L_e}{9525}$ (19) $k_1 = \left(\frac{f'_c}{27.65}\right)^{2/3}$ (20) $k_2 = \frac{d_{frp}-n_e L_e}{d_{frp}}$ (21) $L_e = \frac{25350}{(t_{frp} E_{frp})^{0.58}}$ (22)	$\rho_{frp} = \left(\frac{2t_{frp}}{b_w}\right)$	$R = \alpha\lambda_1\left[\frac{f_c'^{2/3}}{\rho_{frp} E_{frp}}\right]^{\lambda_2}$ (17) $\lambda_1 = \begin{cases} 1.35\; for\; CFRP \\ 1.23\; for\; GFRP \end{cases}$ $\lambda_2 = \begin{cases} 0.30\; for\; CFRP \\ 0.47\; for\; GFRP \end{cases}$ $V_r \leq V_c + 0.8\lambda\emptyset_c\sqrt{f'_c} b_w d$ (23)
Model 4 [20-21]	$V_{FRP} = 2\, f_{FRP,e}\, t_{FRP} w_{FRP} \frac{h_{FRP,e}}{s_{FRP}} (cot\theta + cot\beta)sin\beta$ (24) $f_{FRP,e} = D_{FRP}\sigma_{FRP,max}$ (25)	$L_{max} = \frac{h_{FRP,e}}{sin\beta}$, $h_{FRP,e} = 0.9 \cdot d$ $D_{FRP} = \begin{cases} \frac{2}{\pi\lambda}\frac{1-cos\frac{\pi}{2}\lambda}{sin\frac{\pi}{2}\lambda} \;\; if\; \lambda \leq 1 \\ 1 - \frac{\pi-2}{\pi\lambda} \;\; if\; \lambda > 1 \end{cases}$ (26)	$\sigma_{FRP,max} = min \begin{cases} f_{FRP} \\ 0.427\beta_w\beta_L\sqrt{\frac{E_{FRP}\sqrt{f'_c}}{t_{FRP}}} \end{cases}$ (27)	$\lambda = \frac{L_{max}}{L_e}$ (30) $L_e = \sqrt{\frac{E_{FRP} t_{FRP}}{\sqrt{f'_c}}}$ (31) $\beta_L = \begin{cases} 1 & if\; \lambda \geq 1 \\ sin\frac{\pi\lambda}{2} & if\; \lambda < 1 \end{cases}$ (29) $\beta_w = \sqrt{\frac{2-w_{FRP}/s_{FRP}sin\beta}{1+w_{FRP}/s_{FRP}sin\beta}}$ (28)
Model 5 [22]	$v_f = \frac{A_f f_{fe}(sin\beta+cos\beta)d_f}{s_f}$ (32) $f_{fe} = R f_{fu}$ (33)	$\rho_f = (2t_f/b_w)(w_f/s_f)$ -For U-jacketing: $w_{fe} = d_f - L_e$, - For side bonding: $w_{fe} = d_f - 2L_e$ $L_e = e^{6.134-0.58ln(t_f E_f)}$ (37)	$s_f = w_f$ The spacing s_f and width w_f of the FRP strips should be determined as shown in Figure 14, specifically when the fibers are arranged in a strip configuration.	R is a reduction factor determined by the following equations: $R_1 = 0.5622(\rho_f E_f)^2 - 1.2188(\rho_f E_f) + 0.778$ (34) $R_2 = \frac{0.0042(f_c)^{2/3} w_{fe}}{(t_f E_f)^{0.58}\varepsilon_{fu} d_f}$ (35) The final R value is the smallest limit between $R_1, R_2, and\; R_3 = 0.5$ (36) ensuring conservative predictions.

TABLE IV. PREDICTION OF SHEAR STRENGTH PROVIDED BY FRP

a/d ratio	Beam specimen	$V_f(exp)$ (kN)	Model 1 [19]		Model 2 [23]		Model 3 [24]		Model 4 [20-21]		Model 5 [22]	
			V_f $(pred)$	$\frac{V_f(\text{exp})}{V_f(\text{pred})}$	V_f $(pred)$	$\frac{V_f(\text{exp})}{V_f(\text{pred})}$	V_f $(pred)$	$\frac{V_f(\text{exp})}{V_f(\text{pred})}$	V_f $(pred)$	$\frac{V_f(\text{exp})}{V_f(\text{pred})}$	V_f $(pred)$	$\frac{V_f(\text{exp})}{V_f(\text{pred})}$
2.8	$BS_2 – S_0$ - R2.8	34	23.4	1.4	32	1.1	13.7	2.46	39.6	0.853	30.7	1.1
	$BS_4 – S_0$ - R2.8	37	46.7	0.8	42	0.9	27.5	1.4	53	0.70	49.2	0.8
2.4	$BS_2 – S_0$ - R2.4	26	23.4	1.1	32	0.9	13.7	1.87	39.6	0.65	30.7	0.8
	$BS_4 – S_0$ - R2.4	35	46.7	0.8	42	0.9	27.5	1.3	53	0.66	49.2	0.7

REFERENCES

[1] S.-W. Bae and A. Belarbi, "Behavior of Various Anchorage Systems Used for Shear Strengthening of Concrete Structures with Externally Bonded FRP Sheets," *Journal of Bridge Engineering*, vol. 18, no. 9, pp. 837–847, Sep. 2013, https://doi.org/10.1061/(ASCE)BE.1943-5592.0000420.

[2] R. Kalfat, R. Al-Mahaidi, and S. T. Smith, "Anchorage Devices Used to Improve the Performance of Reinforced Concrete Beams Retrofitted with FRP Composites: State-of-the-Art Review," *Journal of Composites for Construction*, vol. 17, no. 1, pp. 14–33, Feb. 2013, https://doi.org/10.1061/(ASCE)CC.1943-5614.0000276.

[3] A. K. Panigrahi, K. C. Biswal, and M. R. Barik, "Strengthening of shear deficient RC T-beams with externally bonded GFRP sheets," *Construction and Building Materials*, vol. 57, pp. 81–91, Apr. 2014, https://doi.org/10.1016/j.conbuildmat.2014.01.076.

[4] H. A. Al-Baghdadi and A. Sabah, "Behavior of RC Beams Strengthened with NSM-CFRP Strips Subjected to Fire Exposure: A Numerical Study," *Engineering, Technology & Applied Science Research*, vol. 11, no. 6, pp. 7782–7787, Dec. 2021, https://doi.org/10.48084/etasr.4493.

[5] O. A. Hussein and N. N. Khalid, "Behavior of slender RC columns strengthened with partial and full wrapping of BFRP sheet, subjected to variable eccentric loading," *Journal of Building Pathology and Rehabilitation*, vol. 9, no. 1, Jun. 2024, Art. no. 48, https://doi.org/10.1007/s41024-024-00396-5.

[6] E. Monaldo, F. Nerilli, and G. Vairo, "Basalt-based fiber-reinforced materials and structural applications in civil engineering," *Composite Structures*, vol. 214, pp. 246–263, Apr. 2019, https://doi.org/10.1016/j.compstruct.2019.02.002.

[7] R. Madotto, N. C. Van Engelen, S. Das, G. Russo, and M. Pauletta, "Shear and flexural strengthening of RC beams using BFRP fabrics," *Engineering Structures*, vol. 229, Feb. 2021, Art. no. 111606, https://doi.org/10.1016/j.engstruct.2020.111606.

[8] A. Bastani, S. Das, and D. Lawn, "Rehabilitation of Shear Deficient Steel Beams Using BFRP Fabric," *Structures*, vol. 19, pp. 349–361, Jun. 2019, https://doi.org/10.1016/j.istruc.2019.01.019.

[9] J. Sim, C. Park, and D. Y. Moon, "Characteristics of basalt fiber as a strengthening material for concrete structures," *Composites Part B: Engineering*, vol. 36, no. 6–7, pp. 504–512, Jan. 2005, https://doi.org/10.1016/j.compositesb.2005.02.002.

[10] V. Fiore, T. Scalici, G. Di Bella, and A. Valenza, "A review on basalt fibre and its composites," *Composites Part B: Engineering*, vol. 74, pp. 74–94, Jun. 2015, https://doi.org/10.1016/j.compositesb.2014.12.034.

[11] Q. A. Hassan, A. M. Jabbar, and D. H. Mohammed, "Experimental and Numerical Investigation of the Impact of Basalt Fibers and Tie Spacing on Short Concrete Column Behavior," *International Journal of Engineering*, vol. 36, no. 7, pp. 1287–1299, 2023, https://doi.org/10.5829/IJE.2023.36.07A.10.

[12] S. Kar and K. C. Biswal, "External shear strengthening of RC beams with basalt fiber sheets: An experimental study," *Structures*, vol. 31, pp. 305–315, Jun. 2021, https://doi.org/10.1016/j.istruc.2021.01.094.

[13] A. Saribiyik, B. Abodan, and M. T. Balci, "Experimental study on shear strengthening of RC beams with basalt FRP strips using different wrapping methods," *Engineering Science and Technology, an International Journal*, vol. 24, no. 1, pp. 192–204, Feb. 2021, https://doi.org/10.1016/j.jestch.2020.06.003.

[14] W. Zhang, S. Kang, Y. Huang, and X. Liu, "Behavior of Reinforced Concrete Beams without Stirrups and Strengthened with Basalt Fiber–Reinforced Polymer Sheets," *Journal of Composites for Construction*, vol. 27, no. 2, Apr. 2023, Art. no. 04023007, https://doi.org/10.1061/JCCOF2.CCENG-4082.

[15] Iraqi Specifications No. 5: *Portland Cement*. Iraq: Central Agency for Standardization and Quality Control, 2019.

[16] Iraqi Specifications No. 45: *The Used Aggregate from Natural Sources in Concrete and Building*. Iraq: Central Agency for Standardization and Quality Control, 1984.

[17] ASTM C1240-05, *Standard Specification for Silica Fume Used in Cementitious Mixtures*. West Conshohocken, PA, USA: ASTM International, 2005.

[18] ASTM C496/C496M-99a, *Standard Test Method for Splitting Tensile Strength of Cylindrical Concrete Specimens*. West Conshohocken, PA, USA: ASTM International, 2005.

[19] ACI 440.2R-17, *Guide for the Design and Construction of Externally Bonded FRP Systems for Strengthening Concrete Structures*, American Concrete Institute, Farmington Hills, MI, USA, 2017.

[20] J. F. Chen and J. G. Teng, "Shear capacity of FRP-strengthened RC beams: FRP debonding," *Construction and Building Materials*, vol. 17, no. 1, pp. 27–41, Feb. 2003, https://doi.org/10.1016/S0950-0618(02)00091-0.

[21] J. F. Chen and J. G. Teng, "Shear Capacity of Fiber-Reinforced Polymer-Strengthened Reinforced Concrete Beams: Fiber Reinforced Polymer Rupture," *Journal of Structural Engineering*, vol. 129, no. 5, pp. 615–625, May 2003, https://doi.org/10.1061/(ASCE)0733-9445(2003)129:5(615).

[22] A. Khalifa, W. J. Gold, A. Nanni, and A. A. M.I., "Contribution of Externally Bonded FRP to Shear Capacity of RC Flexural Members," *Journal of Composites for Construction*, vol. 2, no. 4, pp. 195–202, Nov. 1998, https://doi.org/10.1061/(ASCE)1090-0268(1998)2:4(195).

[23] T. Triantafillou and International Federation for Structural Concrete, Eds., *Externally bonded FRP reinforcement for RC structures: technical report on the design and use of externally bonded fibre reinforced polymer reinforcement (FRP EBR) for reinforced concrete structures*. Lausanne: International Federation for Structural Concrete, 2001.

[24] ISIS Canada, *Educational Module No. 4: An Introduction to FRP-Strengthening of Concrete Structures*, Dept. of Civil Engineering, Queen's University, Feb. 2004.